Stem Cell Research & Therapy

RESEARCH

Open Access

Clusterin-carrying extracellular vesicles derived from human umbilical cord mesenchymal stem cells restore the ovarian function of premature ovarian failure mice through activating the PI3K/AKT pathway

Jing He[1], Chunchun Ao[1], Mao Li[2], Taoran Deng[3], Shuo Zheng[4], Ke Zhang[1], Chengshu Tu[5], Yu Ouyang[1], Ruibo Lang[1], Yijia Jiang[1], Yifan Yang[1], Changyong Li[6,7*] and Dongcheng Wu[1,4,8*]

Abstract

Background Emerging evidence has highlighted the therapeutic potential of human umbilical cord mesenchymal stem cells (UC-MSCs) in chemotherapy-induced premature ovarian failure (POF). This study was designed to investigate the appropriate timing and molecular mechanism of UC-MSCs treatment for chemotherapy-induced POF.

Methods Ovarian structure and function of mice were assessed every 3 days after injections with cyclophosphamide (CTX) and busulfan (BUS). UC-MSCs and UC-MSCs-derived extracellular vesicles (EVs) were infused into mice via the tail vein, respectively. Ovarian function was analyzed by follicle counts, the serum levels of hormones and ovarian morphology. The apoptosis and proliferation of ovarian granulosa cells were analyzed in vitro and in vivo. Label-free quantitative proteomics was used to detect the differentially expressed proteins in UC-MSC-derived EVs.

Results After CTX/BUS injection, we observed that the ovarian function of POF mice was significantly deteriorated on day 9 after CTX/BUS infusion. TUNEL assay indicated that the number of apoptotic cells in the ovaries of POF mice was significantly higher than that in normal mice on day 3 after CTX/BUS injection. Transplantation of UC-MSCs on day 6 after CTX/BUS injection significantly improved ovarian function, enhanced proliferation and inhibited apoptosis of ovarian granulosa cells, whereas the therapeutic effect of UC-MSCs transplantation decreased on day 9, or day 12 after CTX/BUS injection. Moreover, EVs derived from UC-MSCs exerted similar therapeutic effects on POF. UC-MSCs-derived EVs could activate the PI3K/AKT signaling pathway and reduce ovarian granulosa cell apoptosis. Quantitative proteomics analysis revealed that clusterin (CLU) was highly expressed in the EVs of UC-MSCs. The supplementation of CLU proteins prevented ovarian granulosa cells from chemotherapy-induced apoptosis. Further mechanistic analysis showed that CLU-knockdown blocked the PI3K/AKT signaling and reversed the protective effects of UC-MSCs-derived EVs.

Conclusions Administration of UC-MSCs and UC-MSCs-derived EVs on day 6 of CTX/BUS injection could effectively improve the ovarian function of POF mice. UC-MSCs-derived EVs carrying CLU promoted proliferation and inhibited

*Correspondence:
Changyong Li
lichangyong@whu.edu.cn
Dongcheng Wu
bcdcwu@hotmail.com
Full list of author information is available at the end of the article

apoptosis of ovarian granulosa cells through activating the PI3K/AKT pathway. This study identifies a previously unrecognized molecular mechanism of UC-MSCs-mediated protective effects on POF, which pave the way for the use of cell-free therapeutic approach for POF.

Keywords POF, UC-MSCs, EVs, Clusterin, PI3K/AKT

Graphical Abstract

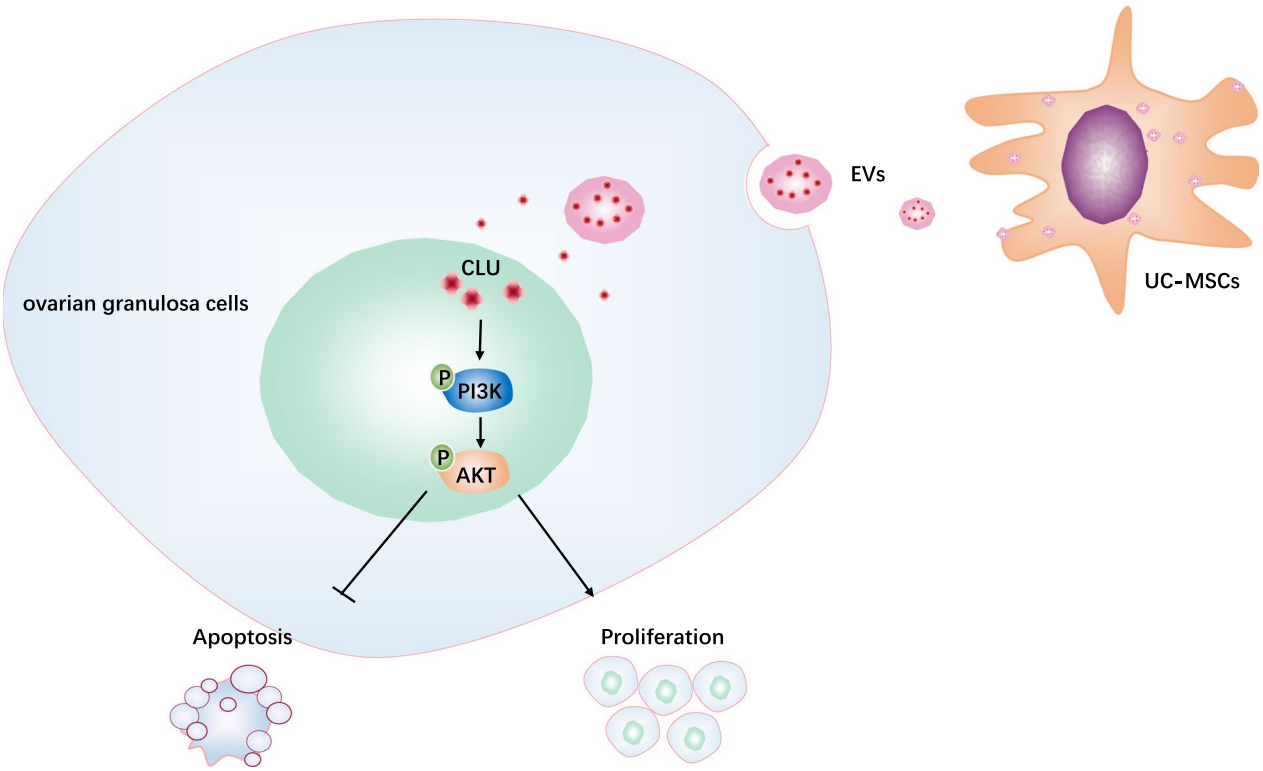

Introduction

Premature ovarian failure (POF) is an ovarian defect characterized by markedly reduced ovarian reserves in women aged less than 40 years [1, 2]. The incidence of POF has been reported to be 1% in females under the age of 40 years [3]. Chemotherapy and/or radiation therapy can lead to apoptosis of normal cells and damage the reproductive system, which have become common and important causes of POF in young cancer patients [4]. Hormone replacement therapy (HRT) is the primary treatment for POF-related symptoms including either estrogen therapy or a combination of estrogen and progesterone therapy [5]. However, HRT can only relieve menopausal symptoms, slow deterioration, fail to repair damaged ovarian tissue [6–8].

During the past few years, mesenchymal stem cells (MSCs) therapy has attracted increasingly more attention due to their potential to restore ovarian structure and function [9–11]. Several reports have shown that human umbilical cord MSCs (UC-MSCs) can be used for improving ovarian function and restoring serum sex hormone levels, as well as inhibiting apoptosis of ovarian tissue [12, 13]. Meanwhile, increasing evidence suggests that paracrine signaling plays a role in the therapeutic efficacy of UC-MSCs. Extracellular vesicles (EVs), membranous structures secreted by cells, have emerged as major paracrine effectors. EVs include exosomes (with a diameter ranging from 30 to 150 nm), microcapsules (200–500 nm in diameter), and apoptotic bodies (exceeding 1000 nm in diameter) [14]. In addition, EVs have been identified as important messengers between cells, delivering functional molecules such as microRNAs, long noncoding RNAs, and proteins to recipient cells [15, 16]. Several studies have indicated that EVs promoted angiogenesis, attenuated cell apoptosis and restore ovarian function via transferring functional miRNAs or proteins

[4, 17, 18]. Nevertheless, the efficacy of UC-MSCs in preclinical and clinical studies of POF is not always satisfactory, with results varying dependent on the timing of administration in different studies. Meanwhile, the potential mechanisms of the protection provided by UC-MSCs and UC-MSCs-derived EVs in POF have not been elucidated. Based on the above findings, we speculate that UC-MSCs may restore the ovarian function of POF mice by transferring EVs-containing proteins.

Here, we aimed to identify the pathological changes in the ovaries of mice with chemotherapeutic drug-induced POF over time and further explore the appropriate timing of UC-MSCs or UC-MSCs-derived EVs therapy. Meanwhile, we characterized the proteome profiles of UC-MSCs-derived EVs and explored the underlying molecular mechanism of UC-MSCs-derived EVs in restoring ovarian function.

Materials and methods

Isolation, culture, and identification of UC-MSCs

The utilization of human umbilical cord tissue was endorsed by the Institutional Ethics Review Board of Renmin Hospital of Wuhan University (Permit Number: WDRY2019-G001). Informed consent was obtained from all participants. The umbilical cord tissue was sterilized with 75% alcohol, followed by multiple rinses with phosphate-buffered saline (PBS). After removing the umbilical vein and artery, the tissue was cut into small pieces and evenly tiled on the sterile culture dishes. The dishes were supplemented with serum-free stem cell culture medium (YoCon, Beijing, China), and placed in a 37 °C, 5% CO_2 incubator. The culture medium was renewed at intervals of 2–3 days. Cells were trypsinized and passaged until they reached 80–90% confluence. After the fourth generation of cells was cultured for 72 h, the supernatant was collected as UC-MSC-conditioned medium (MSC-CM) for subsequent experiments. GW4869 has been widely used for inhibiting the secretion of EVs. When the fourth generation of cells reached a confluence level of 70–80%, the culture medium was replaced with fresh medium containing GW4869 (10 μM), and the supernatant was collected after 24 h as GW4869-CM for subsequent experiments.

UC-MSCs were analyzed for surface markers using the Human MSC Analysis Kit (562,245, BD Biosciences, NJ, USA). Lipogenic, osteogenic, and chondrogenic differentiation of UC-MSCs were performed to verify the differentiation potential of the MSCs using specialized inducers (6114531, 6114541, and 6114551, DAKEWE, Shenzhen, China). Alizarin Red, Alcian Blue and Oil Red O stainings were used to identify osteoblasts, adipocytes, and chondrocytes, respectively.

Preparation and identification of UC-MSCs-derived EVs

The MSC-CM was sequentially centrifuged at 300 g, 2000 g, and 10,000 g to remove large particles and cell debris. The supernatant was transferred to a 100 kDa MWCO ultrafiltration tube (UFC9050, Merck, USA) and centrifuged at 5000 g for 30 min to collect the concentrated solution above the membrane. After that, the collected solution was centrifuged at 100,000 g for 70 min to remove the supernatant. The centrifugation process was repeated once and the pellet resuspended in an appropriate volume of PBS. The entire experiment was conducted at 4 °C.

The size and particle concentration of EVs were analyzed using nanoparticle tracking analysis (NTA). Additionally, the morphology of EVs was evaluated using transmission electron microscopy (TEM). Western blotting was employed to confirm the expression of related markers (CD9, Alix) and negative control (Calnexin). The dose of EVs derived from UC-MSCs was quantitatively determined by bicinchoninic acid assay (BCA) protein assay.

Animals

Seven-week-old female specific pathogen-free (SPF level) C57/BL6 mice (Hubei Provincial Center for Disease Control and Prevention, Wuhan) were used in this study. All animal experiments were approved by the Committee of Animal Care and Use of Hubei Provincial Center for Food and Drug Safety Evaluation and Animal Experiment (Permit Number: 202210022) and the Bestcell Model Biological Center Notification of the Result for Ethical Approval for Research Involving Animals (The permit Number: BSMS 2022-06-27A). All animal experiments were complied with the guidelines for the care and use of laboratory animals. All the animals were allowed free access to distilled water, standard food and were housed under standard feeding conditions (temperature 20 ± 2 °C; humidity 45–55%; 12 h light & dark cycle). Mice were randomly divided into 4–5 mice per cage. The animals were excluded if the animal died prematurely, preventing the collection of behavioral and histological data.

Animal model

POF was induced in female C57BL/6 mice by intraperitoneal injections with busulfan (BUS, 30 mg/kg, MedChemexpress, NJ, USA) and cyclophosphamide (CTX, 120 mg/kg, Sigma-Aldrich, MO, USA). Mice were randomly divided into two groups (34 mice/group), with four or five mice per group (NC and POF groups) were sacrificed at 3, 6, 9, 12, 15, 18, and 21 days after injection.

The POF mice receiving UC-MSCs (5 per group) were injected with 200 μL PBS containing UC-MSCs (2×10^7 cells/kg) via tail vein on days 6, 9, and 12 after CTX and BUS treatment, respectively. Mice (5 per group) undergoing EVs treatment were injected with 200 μL of PBS containing 75 μg EVs by tail vein on day 6. All mice were examined for estrous cycles 3 weeks after CTX/BUS injection and were sacrificed when they were in diestrus phase. The test time was between 09.30 and 11.30 am and testing order was randomized daily. Mice serum was sampled by extracting the eyeball blood after mice were anesthetized with 1% pentobarbital sodium. After that, all mice were euthanized by cervical dislocation. The animals were included in the study if they underwent successful UC-MSCs or UC-MSCs-derived EVs injection. All study personnel were blind to treatment allocation and had no way of influencing whether an animal would receive PBS, UC-MSCs or EVs derived from UC-MSCs.

Ovarian morphology analysis and follicle counts

The ovaries were collected and fixed with tissue fixation solution (B0038, Powerful biology). The fixed ovaries were dehydrated, embedded in paraffin, and cut into 5 μm sections for hematoxylin and eosin (HE) staining and immunofluorescence analysis. The ovarian tissue morphology was observed using an optical microscope (Olympus Corporation, Tokyo, Japan), and the number of follicles at different stages, including primordial, primary, secondary, and atretic, were counted [19, 20]. Three sections were analyzed for each tissue sample from n = 4–5 mice per group.

Immunofluorescence assay

Ovarian tissue sections were fixed and incubated with 3% bovine serum albumin (BSA) for 30 min at 37 °C. Subsequently, the sections were incubated with primary antibodies against cleaved-caspase3 (1:400) (#9661, CST, MA, USA) or proliferating cell nuclear antigen (PCNA) (1:200) (GB12010, Servicebio, Wuhan, China). After washing with PBS, the sections were incubated with secondary antibodies at 37 °C for 1 h. DAPI staining was performed (Servicebio, Wuhan, China), and images were detected using a laser scanning confocal microscope (Nikon Corporation, Tokyo, Japan).

TdT mediated dUTP nick end labeling (TUNEL) assay

According to the manufacturer's instructions, the TUNEL apoptosis assay kit (Servicebio, Wuhan, China) was used to detect apoptotic cells in ovarian tissue sections from different groups, followed by quantitative analysis.

Hormone assay

Blood samples were collected from mice and centrifuged at 2000 rpm for 20 min at 4 °C. Serum levels of E2, and FSH were measured using ELISA kits following the manufacturer's instructions.

Cell culture and treatment

Human ovarian granulosa cells (KGN cell line) and human renal epithelial cells (HEK293T cell line) were purchased from the China Center for Type Culture Collection (Wuhan China). KGN cells were cultured in Dulbecco's modified Eagle's medium (DMEM, Gibco, NY, USA) containing 5% fetal bovine serum (FBS, Gibco, NY, USA), while HEK293T cells were cultured in DMEM medium supplemented with 10% FBS at 37 °C and 5% CO_2 concentration in a humidified atmosphere. Following 72 h of incubation, when the cell fusion efficiency reached 80–90%, the supernatant was collected as KGN-CM and 293 T-CM for subsequent experiments.

An ovarian granulosa cell injury model was established by treating KGN cells with 5 μg/mL nitrogen mustard (NM) (mechlorethamine hydrochloride, Macklin, Shanghai, China) for 48 h in vitro. KGN cells were seeded at 3×10^4 cells in 6-well plates. After 24 h, these cells were exposed to media with 50% various supernatant, respectively. Subsequently, co-cultures were incubated for 48 h with NM.

Annexin-V-FITC and propidium iodide staining

According to the manufacturer's instructions, cells from different groups were collected, washed twice with PBS, and resuspended. Cells were then stained with Annexin V-FITC/PI Apoptosis Detection Kit (C1062, Beyotime Biotechnology, China) for 20 min. Finally, the apoptotic cell rate was determined using flow cytometry.

CCK-8 assay

KGN cells were seeded at 3000 cells in 96-well plates. After replacing the medium, NM was added to induce the cells for 24 h, and their growth was measured after adding 10 μL CCK-8 into the culture medium for 1.5 h. The optical density (OD) value at 450 nm was determined.

siRNA transfection

Cells were seeded into a 6-well plate at a density of 1×10^5 cells per well. For small interfering RNA (siRNA)-mediated gene knockdown, 100 nM of siRNA was transfected into the cells using an EL (TransGen Biotech, China) transfection reagent, according to the

manufacturer's protocols. The culture medium was changed after 6 h. The supernatant was harvested as siNC-CM and siCLU-CM 48 h post-transfection and filtered through a 0.22 um sterile filter. The siRNAs were synthesized by the Ribobio (Guangzhou, China). siCLU: 5′-GCATCATAGACGAGCTCTT-3′. siNC: 5′-TTCTCCGAACGTGTCACGT-3′.

Western blotting

Protein was obtained through lysis of cells using radioimmunoprecipitation assay buffer (P0013C, Beyotime, China), supplemented with a mixture of protease inhibitors and phosphatase inhibitors. Protein concentration was analyzed using the bicinchoninic acid assay (BCA, P0009, Beyotime Biotechnology, China). The proteins were then separated by 10% sodium dodecyl sulfate–polyacrylamide gel electrophoresis (SDS-PAGE) and transferred onto a polyvinylidene difluoride (PVDF) membrane. The membrane was incubated with 5% BSA in Tris-buffered saline with 0.5% Tween-20 to block nonspecific binding. Primary antibodies against BAX (50,599–2-Ig, Proteintech, USA), BCL-XL (2764 s, CST, USA), cleaved-caspase 3 (9661 s, CST, USA), P-AKT (4060 s, CST, USA), AKT (46,917, CST, USA), P-PI3K (ab278545, abcam, UK), PI3K (4257, CST, USA), and β-actin (81,115–1-RR, Proteintech, USA) were incubated with the membrane overnight at 4 °C at an appropriate dilution (1:1000). After washing three times, secondary antibodies were added to the membrane and incubated at RT for 1 h. The chemiluminescent signal was detected using an enhanced chemiluminescence kit (Absin, CN). The results were analyzed using Image J software.

RNA extraction and real-time PCR analysis

Total RNA was extracted from cultured cells with Trizol (15596-018, Invitrogen, USA), reverse-transcribed into cDNA with a reagent kit (RR047B, Takara, China), and amplified by qRT-PCR (CFX connect, Bio-Rad, USA) according to manufacturer's instructions. H-CLU-F: 5′-AAACGAAGAGCGCAAGACAC-3′. H-CLU-R: 5′-TGTTTCAGGCAGGGCTTACA-3′.

Quantitative proteomics analysis

EVs were subjected to Label-free quantification protein profiling, with the culture medium (Control) was designed as the negative control. All protein samples were prepared in triplicates for each biological replicate. The experiment was performed at Wuhan Biobank company (China). Mass spectrometry data were analyzed using MaxQuant software (V1.6.6) with the Andromeda database search algorithm (Cox and Mann 2008; Tyanova, Temu, and Cox 2016). The protein identification was performed against the human protein reference database in Uniprot. Functional annotation and enrichment analysis were conducted using Gene Ontology (GO) (https://www.geneontology.org/), while protein analysis related to metabolic pathways was performed using the Kyoto Encyclopedia of Genes and Genomes (KEGG) database (https://www.genome.jp/KEGG).

Statistical analysis

All data were analyzed using GraphPad Prism 9 software (La Jolla, CA, USA) and were presented as the mean ± standard deviation (SD). Differences between group means were determined with Student's t-test or one-way analysis of variance. $P < 0.05$ was considered statistical significance.

Results

Characterization of UC-MSCs and UC-MSC-derived EVs

The staining results showed that UC-MSCs displayed osteogenic, chondrogenic, and adipogenic differentiation abilities in vitro (Fig. 1A–C). Flow cytometry analysis revealed that UC-MSCs were positive for CD90, CD105 and CD73 but negative for CD11b, CD34, CD19, CD45 and HLA-DR (Fig. 1D). NTA showed that the mean particle diameter of UC-MSC-derived EVs was 121.3 nm (Fig. 1E). Western blotting analysis revealed that the EVs were positive for molecular markers, including Alix, CD9 and TSG101, and negative for Calnexin (Fig. 1F). TEM analysis showed that EVs displayed round nanoparticles ranging from 50 to 200 nm (Fig. 1G).

The structure and function of the ovaries were significantly impaired on day 9 after CTX/BUS injection

After injection of CTX/BUS, the POF mice developed ovarian atrophy over time (Fig. 2A). The changes in the number of follicles showed a clear time-dependent pattern. Compared to that in the control mice, the number of primordial follicles (NC vs. POF, 9.3 ± 0.4 vs. 6.1 ± 0.8) in POF mice decreased significantly after 6 days of CTX/BUS injection. After 9 days of injection, the number of primary follicles (NC vs. POF, 7.8 ± 0.7 vs. 5.0 ± 1.6) and secondary follicles (NC vs. POF, 13.8 ± 5.0 vs. 7.1 ± 1.3) were also significantly decreased. In addition, the number of atretic follicles (NC vs. POF, 0.4 ± 0.1 vs. 1.6 ± 0.1) in POF mice increased significantly on day 3 and remained at high levels (Fig. 2B). Moreover, we found that the E2 concentration (NC vs. POF, 125.7 ± 17.5 pg/mL vs. 86.1 ± 26.9 pg/mL) in POF mice was significantly lower than that of the control mice on day 9 (Fig. 2C), whereas the FSH concentration in POF mice did not show significant change compared with the controls (Fig. 2D). These results suggested that ovarian architecture and function were dramatically impaired in POF mice after 9 days of CTX/BUS injection.

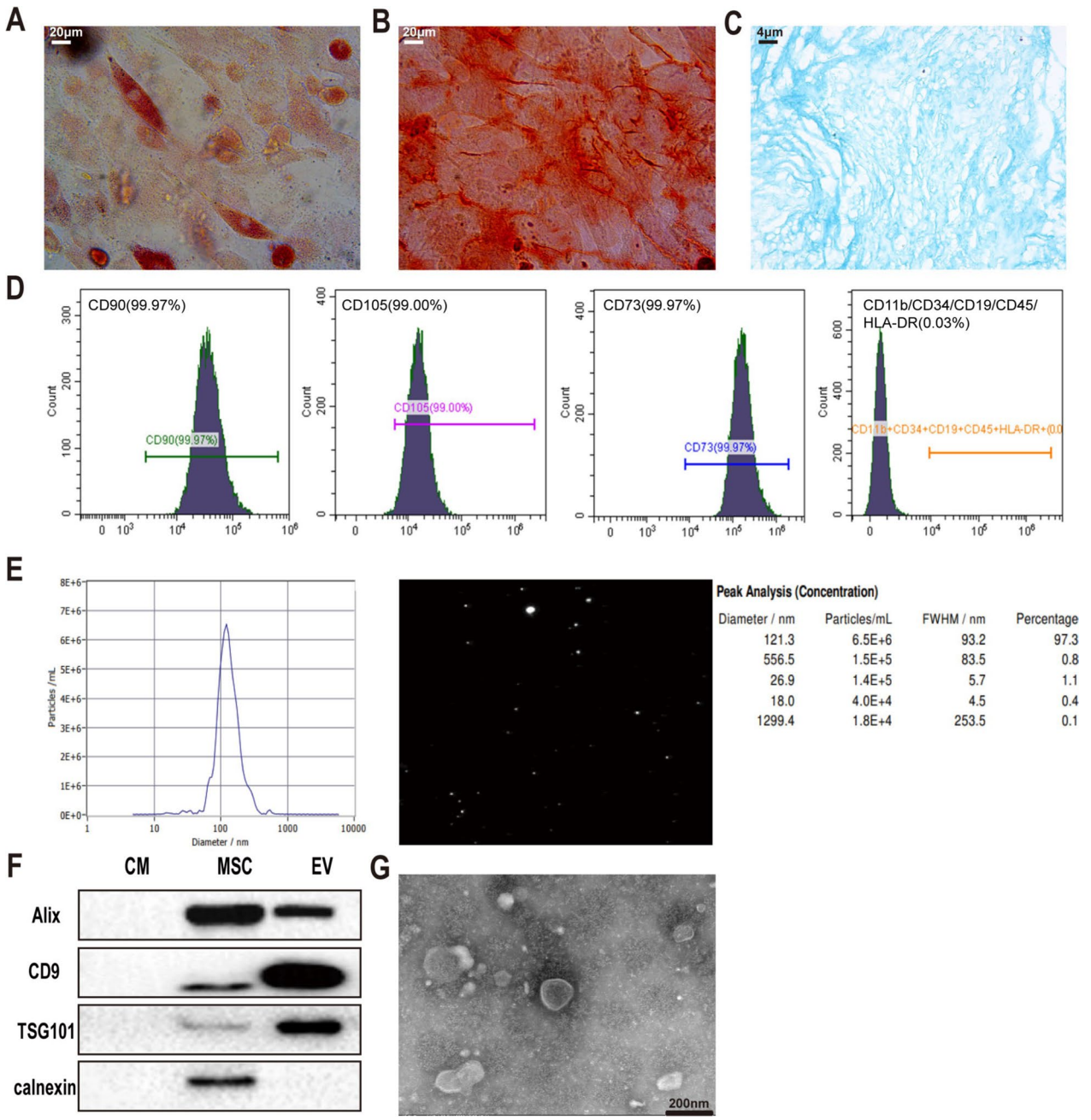

Fig. 1 Identification of human UC-MSCs and UC-MSCs-derived EVs. **A** The adipogenic differentiation was defined by Oil red O staining. Scale bar: 20 μm. **B** The Osteogenic differentiation was determined by Alizarin red staining. Scale bar: 20 μm. **C** The chondrogenic differentiation was defined by Alcian blue staining. Scale bar: 4 μm. **D** Human UC-MSCs were positive for CD73, CD90 and CD105 (more than 99%) but negative for CD11b, CD34, CD19, CD45 and HLA-DR (less than 1%) by flow cytometry. **E** NTA particle size distribution analysis of EVs. **F** Western blot analysis of EVs- specific markers (Alix, Tsg101, and CD9) and cellular marker (Calnexin). The culture medium sample of non-cultured human UC-MSCs were used as a negative control. All full-length blots are presented in Additional file 2: Figure 1F. **G** The morphology and size of EVs under TEM. Scale bar: 200 nm

Apoptosis of ovarian granulosa cells is one of the key phenomena in CTX/BUS-induced POF

In comparison to that in the control mice, TUNEL positive cells (NC vs. POF, $10.1 \pm 3.4/mm^2$ vs. $32.8 \pm 15.0/mm^2$) were markedly increased from day 3 in POF mice (Fig. 3A and C). Notably, we observed that TUNEL-positive cells were primarily ovarian granulosa cells. To determine whether CTX/BUS causes ovarian fibrosis, the

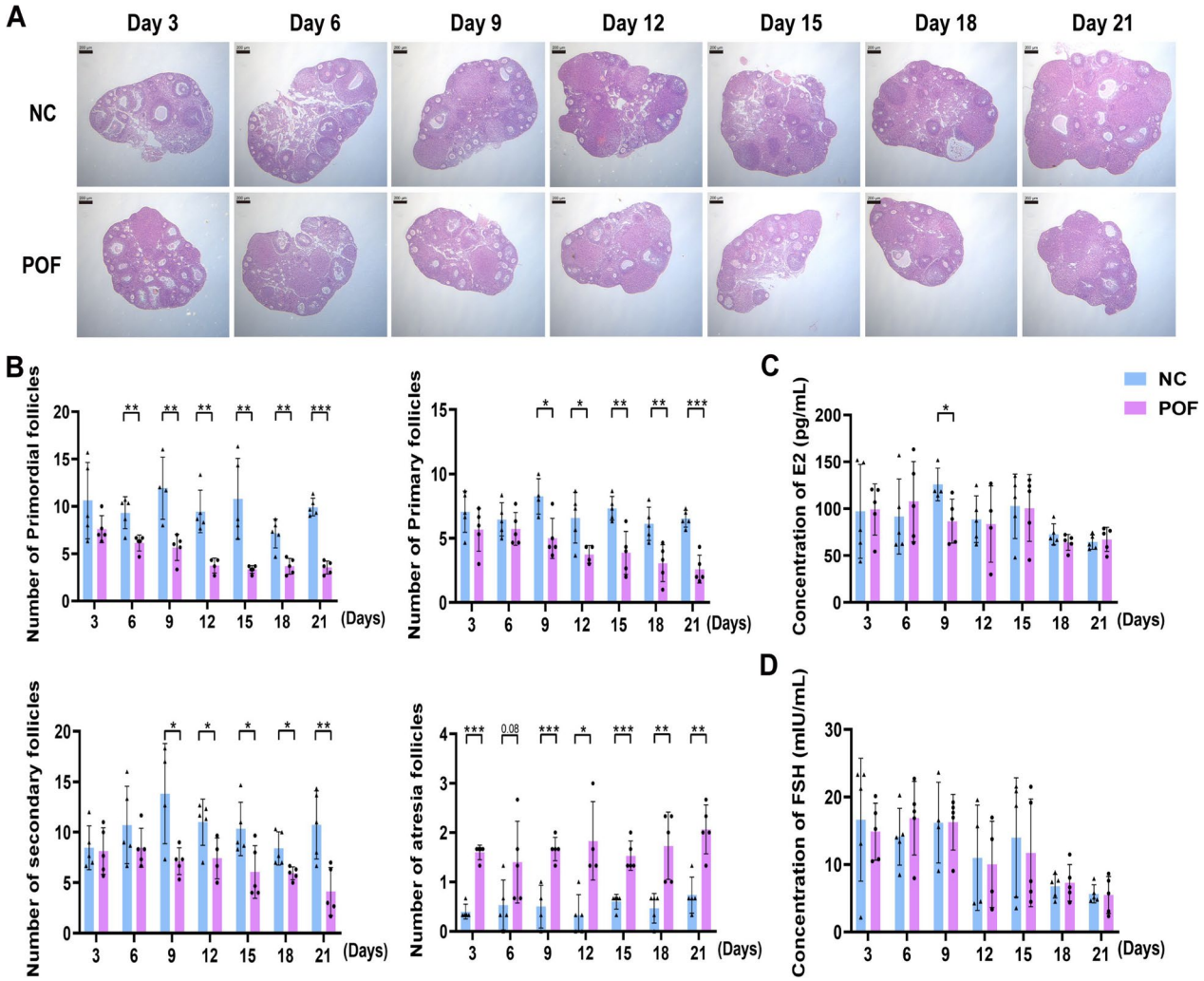

Fig. 2 Time-dependent changes in the number of follicles and hormone levels after CTX/BUS injection. **A** Representative images of HE staining of ovarian tissues. Scale bar: 200 μm. **B** Number of primordial follicles, primary follicles, secondary follicles and atretic follicles at different time points. **C** ELISA for serum levels of E2. **D** ELISA for serum levels of FSH. *$p < 0.05$, **$p < 0.01$, ***$p < 0.001$. $n = 4$–5 per group for all experiments

fibrosis areas of ovarian tissue were examined using Masson staining. The Masson positive areas of ovaries in POF mice were not significantly different from that of the control mice (Fig. 3B and D).

The therapeutic effect of UC-MSCs treatment on day 6 of CTX/BUS injection was significantly better than that on days 9 or 12

Given that the ovarian function was declined significantly on day 9 of CTX/BUS injection, we explored the therapeutic timing of UC-MSCs for POF. The mice were injected intravenously with UC-MSCs (2×10^7 cells/kg) on days 6, 9, and 12 of CTX/BUS injection, respectively. HE staining showed that ovarian atrophy was inhibited in mice treated with UC-MSCs on days 6 and 9. In contrast, no efficacy was observed in POF mice with UC-MSCs on day 12 (Fig. 4A). The number of primordial follicles (POF vs. POF + UC-MSC, 5.0 ± 0.8 vs. 9.5 ± 1.0), primary follicles (POF vs. POF + UC-MSC, 6.8 ± 1.8 vs. 11.1 ± 1.4), secondary follicles (POF vs. POF + UC-MSC, 4.5 ± 1.7 vs. 9.7 ± 1.8) and atretic follicles (POF vs. POF + UC-MSC, 1.3 ± 0.7 vs. 0.3 ± 0.3) was significantly restored by UC-MSCs treatment on day 6 (Fig. 4B). When mice were transplanted with UC-MSCs on day 9, the number of primordial follicles (POF vs. POF + UC-MSC, 5.0 ± 0.8 vs. 7.6 ± 1.7) and secondary follicles (POF vs. POF + UC-MSC, 4.5 ± 1.7 vs. 6.4 ± 0.7) was significantly increased compared to that in the POF mice, however, no difference was observed in the UC-MSCs-treated mice on day 12 (Fig. 4B). Moreover, the E2 concentration was

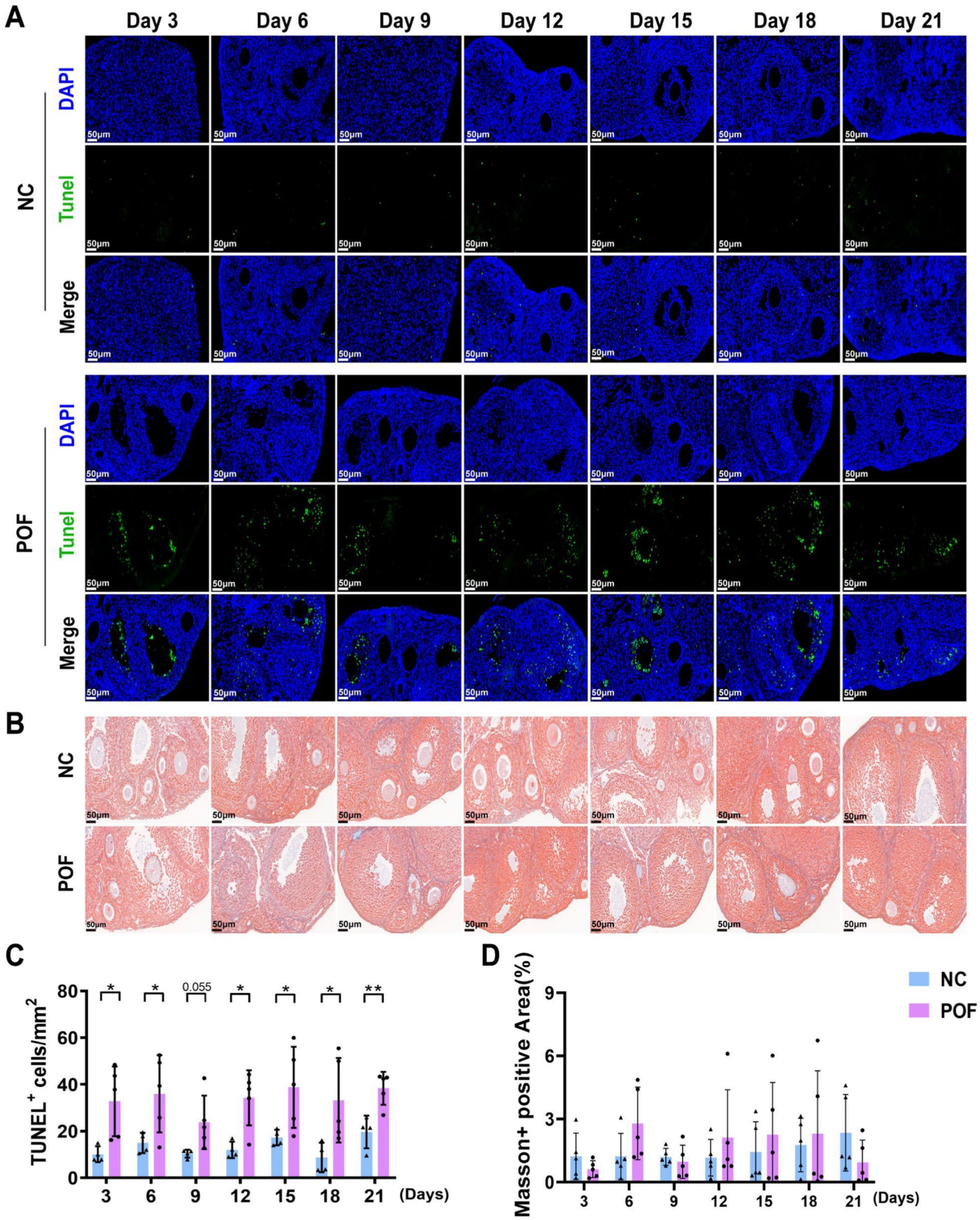

Fig. 3 Changes in apoptosis and fibrosis in ovarian tissue. **A** Representative images of TUNEL staining. Scale bar: 50 μm. **B** Representative images of Masson staining. Scale bar: 50 μm. **C** The quantification of TUNEL assay. **D** The quantification of Masson staining. $^{*}p < 0.05$, $^{**}p < 0.01$. $n = 4–5$ per group for all experiments

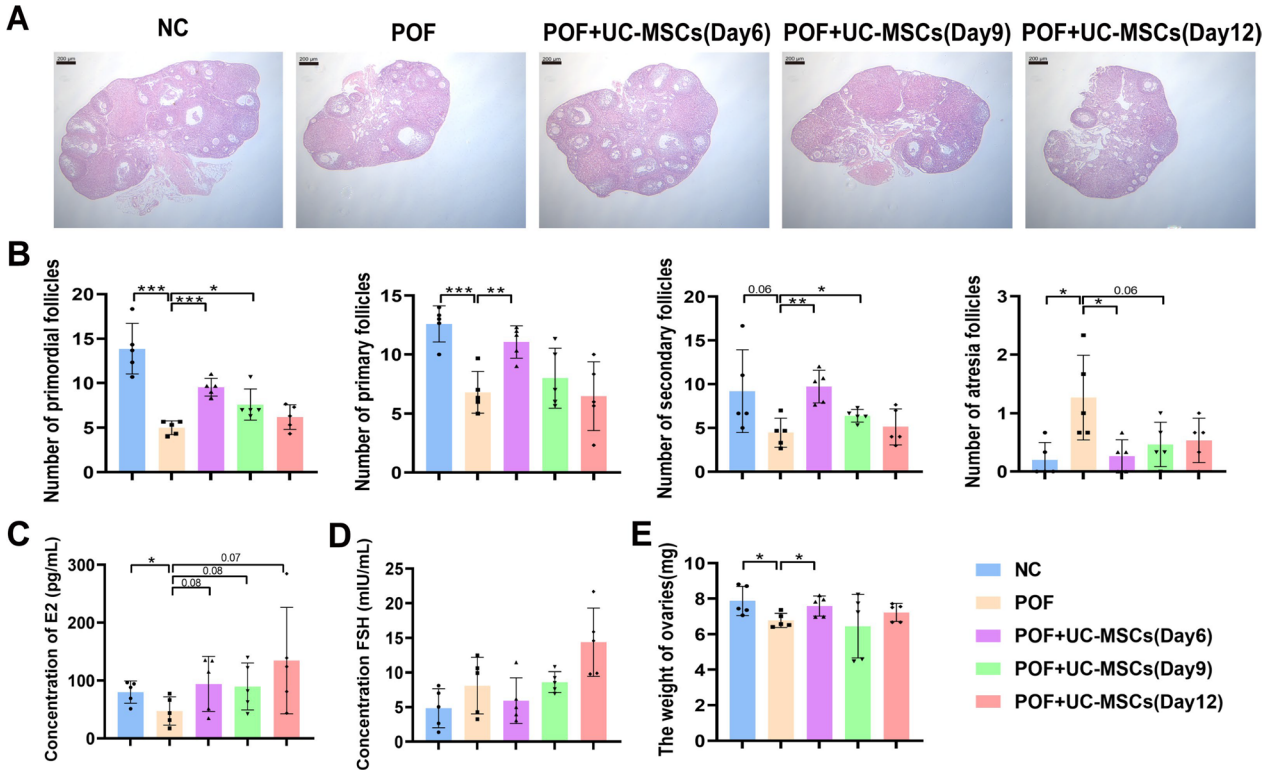

Fig. 4 Therapeutic effects of UC-MSCs in POF mice. **A** Representative images of HE staining. Scale bar: 200 μm. **B** The number of different types of ovarian follicles. (C) ELISA for serum levels of E2. **D** ELISA for serum levels of FSH. **E** The weight of ovaries. *$p < 0.05$, **$p < 0.01$, ***$p < 0.001$. $n = 5$ per group for all experiments

significantly enhanced (POF vs. POF + UC-MSC (Day 6) vs. POF + UC-MSC (Day 9) vs. POF + UC-MSC (Day 12), 47.3 ± 24.6 pg/mL vs. 94.1 ± 47.7 pg/mL vs. 89.6 ± 40.6 pg/mL vs. 134.4 ± 91.9 pg/mL) in the all UC-MSCs-treated mice when compared to the POF mice (Fig. 4C). FSH concentration displayed a decreasing trend in the mice treated with UC-MSCs on day 6 (Fig. 4D). Additionally, the ovarian weight (POF vs. POF + UC-MSC, 6.8 ± 0.4 mg vs. 7.6 ± 0.6 mg) was significantly increased in mice treated with UC-MSCs on day 6 (Fig. 4E).

Meanwhile, TUNEL staining revealed that transplantation of UC-MSCs on day 6 markedly reduced the number of TUNEL-positive cells (POF vs. POF + UC-MSC, 33.1 ± 8.7/mm^2 vs. 17.7 ± 3.3/mm^2) in the ovaries, whereas no notable changes were observed in mice treated on days 9 or 12 (Fig. 5A and C). To investigate whether UC-MSCs promoted the proliferation of ovarian cells, we detected proliferative cells by PCNA immunostaining. The results suggested that treatment with UC-MSCs on day 6 significantly increased the number of PCNA positive cells (POF vs. POF + UC-MSC, 2416 ± 415.4/mm^2 vs. 3321 ± 825.1/mm^2) in POF mice. The same effect was not seen in POF mice treated with UC-MSCs on days 9 or 12 (Fig. 5B and D). Therefore, these findings indicated that UC-MSCs infusion on day 6 inhibited apoptosis and promoted proliferation of ovarian cells in POF mice. Collectively, these results demonstrated that the therapeutic effect of UC-MSCs treatment on day 6 of CTX/BUS injection was significantly better than that on days 9 or 12.

UC-MSC-derived EVs improved ovarian structure and function in POF mice

EVs from UC-MSCs have been reported to have the same therapeutic role as UC-MSCs in disease treatment [15]. We evaluated the role of injection of EVs derived from UC-MSCs in normal and POF mice on the day 6 after CTX/BUS injection. HE staining showed the size of the ovaries was restored by treatment with EVs (Fig. 6A). Consistent with the improved effect of UC-MSCs treatment, EVs derived from UC-MSCs significantly increased the number of primordial follicles (POF vs. POF + EVs, 5.4 ± 0.8 vs. 8.4 ± 1.2), primary follicles (POF vs. POF + EVs, 3.2 ± 0.6 vs. 5.4 ± 1.1), and secondary follicles (POF vs. POF + EVs, 2.5 ± 1.0 vs. 5.0 ± 1.7) and decreased the number of atretic follicles (POF vs. POF + EVs, 1.0 ± 0.5 vs. 0.4 ± 0.2) in POF mice (Fig. 6B). Similarly, UC-MSC-derived EVs promoted

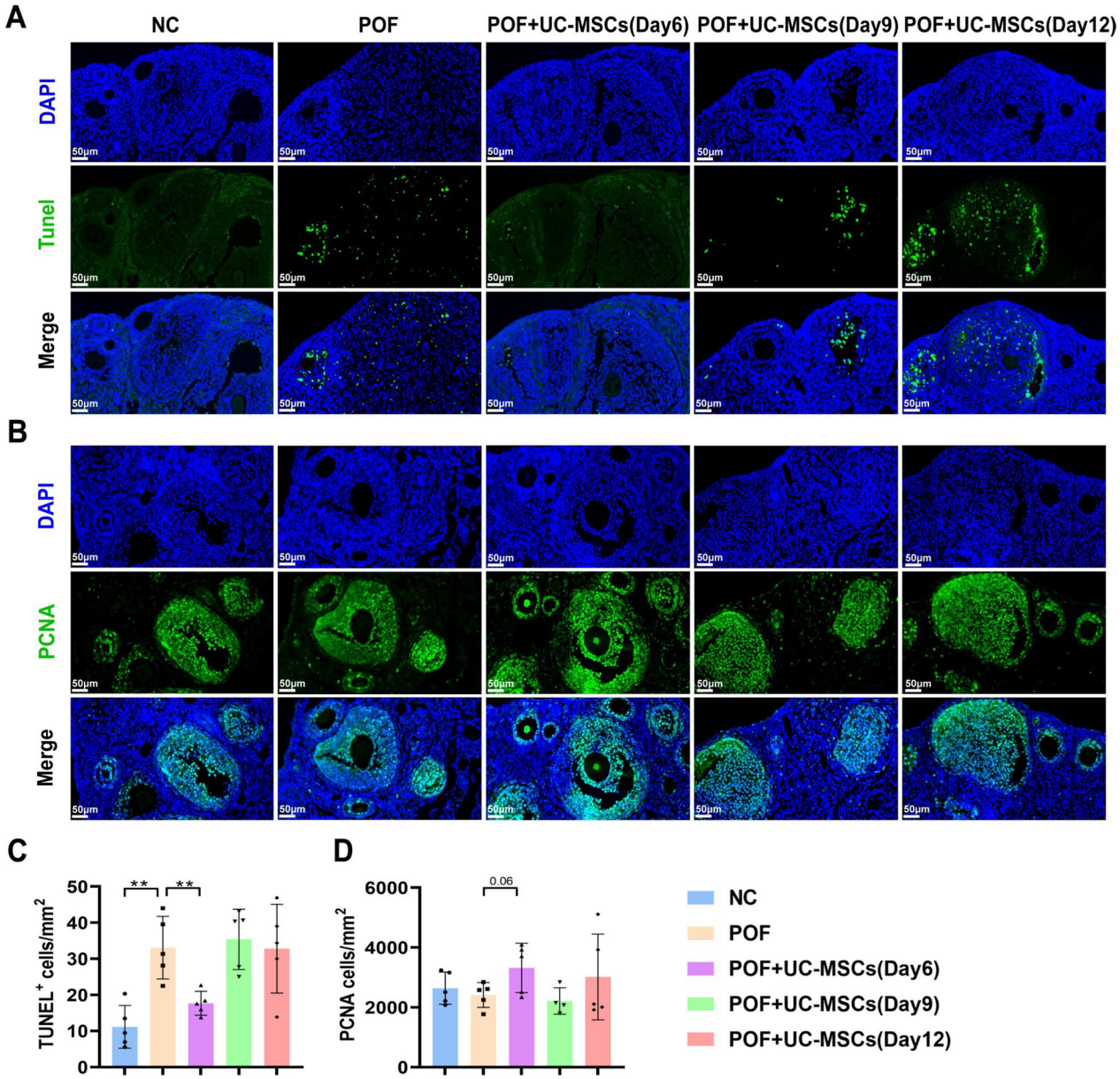

Fig. 5 The anti-apoptotic and pro-proliferative effects of UC-MSC in POF. **A** Representative images of TUNEL staining. Scale bar: 50 μm. **B** Representative images of PCNA immunofluorescence staining. Scale bar: 50 μm. **C** The quantification of TUNEL assay. **D** The quantification of PCNA immunofluorescence. $^{**}p < 0.01$. $n = 5$ per group for all experiments

the recovery of hormones (E2, POF vs. POF + EVs, 56.9 ± 25.5 pg/mL vs. 86.9 ± 14.0 pg/mL; FSH, POF vs. POF + EVs, 32.5 ± 9.3 mIU/mL vs. 16.1 ± 5.6 mIU/mL) and ovarian weight (POF vs. POF + EVs, 5.3 ± 0.9 mg vs. 7.1 ± 0.6 mg) (Fig. 6C–E). Furthermore, UC-MSC-derived EVs did not confer any toxicity to normal mice.

UC-MSC-derived EVs attenuated apoptosis and promoted proliferation in ovarian granulosa cells

We further explored whether UC-MSC-derived EVs protected ovarian granulosa cells against CTX/BUS-induced apoptosis. Compared with those in the POF mice, the administration of EVs led to decreasing the number of TUNEL-positive cells (POF vs. POF + EVs, 107 ± 16.7/mm^2 vs. 37.5 ± 11.5/mm^2) (Fig. 7A). Meanwhile, cleaved-caspase3 expression in the ovaries of POF mice was significantly inhibited by the treatment of EVs (POF vs.

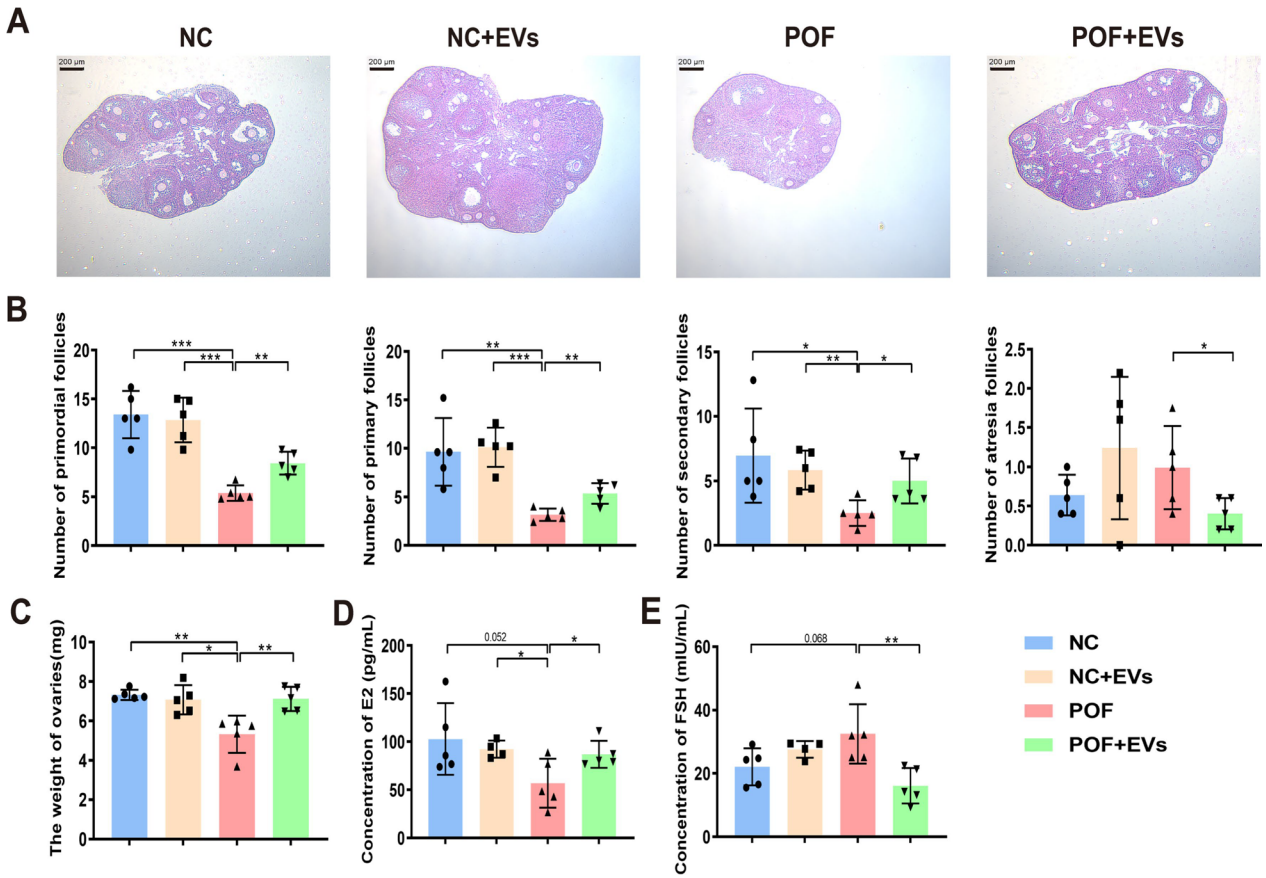

Fig. 6 Therapeutic effects of EVs derived from UC-MSCs in POF mice. **A** Representative images of HE staining. Scale bar: 200 μm. **B** The number of different types of ovarian follicles. **C** The weight of ovaries. **D** ELISA for serum levels of E2. **E** ELISA for serum levels of FSH. $^{*}p < 0.05$, $^{**}p < 0.01$, $^{***}p < 0.001$. $n = 5$ per group for all experiments

POF + EVs, $75.9 \pm 8.2/mm^2$ vs. $18.8 \pm 6.9/mm^2$) (Fig. 7B). Subsequently, we also examined the effect of EVs derived from UC-MSCs on the proliferation of ovarian granulosa cells. An increased number of proliferating cells in the ovaries of mice treated with EVs was observed through PCNA assay analysis (POF vs. POF + EVs, $2281 \pm 604.9/mm^2$ vs. $3659 \pm 333.8/mm^2$) (Fig. 7C). These results showed that EVs derived from UC-MSCs exerted an anti-apoptosis and pro-proliferative effect in the ovaries of POF mice, which was similar to that of UC-MSCs.

UC-MSC-derived EVs inhibited apoptosis and promoted proliferation in KGN cells

Flow cytometry showed that MSC-CM exerted an anti-apoptosis effect in KGN cells (NM vs. NM + MSC-CM, $40.4 \pm 3.2\%$ vs. $20.6 \pm 2.0\%$), but 293 T-CM had no effect (Fig. 8A). In addition, Western Blot analysis indicated that MSC-CM significantly up-regulated the relative protein expression levels of the anti-apoptotic protein BCL-XL and down-regulated pro-apoptotic protein cleaved-caspase3 (Fig. 8C). Activation of the PI3K/AKT signaling pathway is associated with cell proliferative and apoptosis. To investigate whether MSC-CM can activate the PI3K/AKT signaling pathway, we detected the relative protein expression levels of p-PI3K and p-AKT in KGN cells. The inclusion of MSC-CM led to an increase in the protein expression levels of p-PI3K and p-AKT in KGN cells, compared to the treatment with 293 T-CM (Fig. 8C). Furthermore, CCK8 assay indicated that MSC-CM significantly enhanced proliferation of KGN cells (NM vs. NM + MSC-CM, $26.8 \pm 6.2\%$ vs. $43.6 \pm 3.4\%$) (Fig. 8E).

We used the EVs inhibitor (GW4869) to inhibit the secretion of UC-MSC-derived EVs. The anti-apoptotic effect of MSC-CM on KGN cells was reversed by GW4869 pretreatment (NM + MSC-CM vs. NM + GW4869-CM, $23.5 \pm 3.1\%$ vs. $52.4 \pm 5.1\%$) (Fig. 8B and D). Meanwhile, after inhibition of EVs with GW4869, the activation of the PI3K/AKT signaling pathway in KGN cells induced by MSC-CM was suppressed (Fig. 8D). Furthermore, the inhibition of EVs significantly impaired the proliferative effect of MSC-CM on KGN cells (NM + MSC-CM vs.

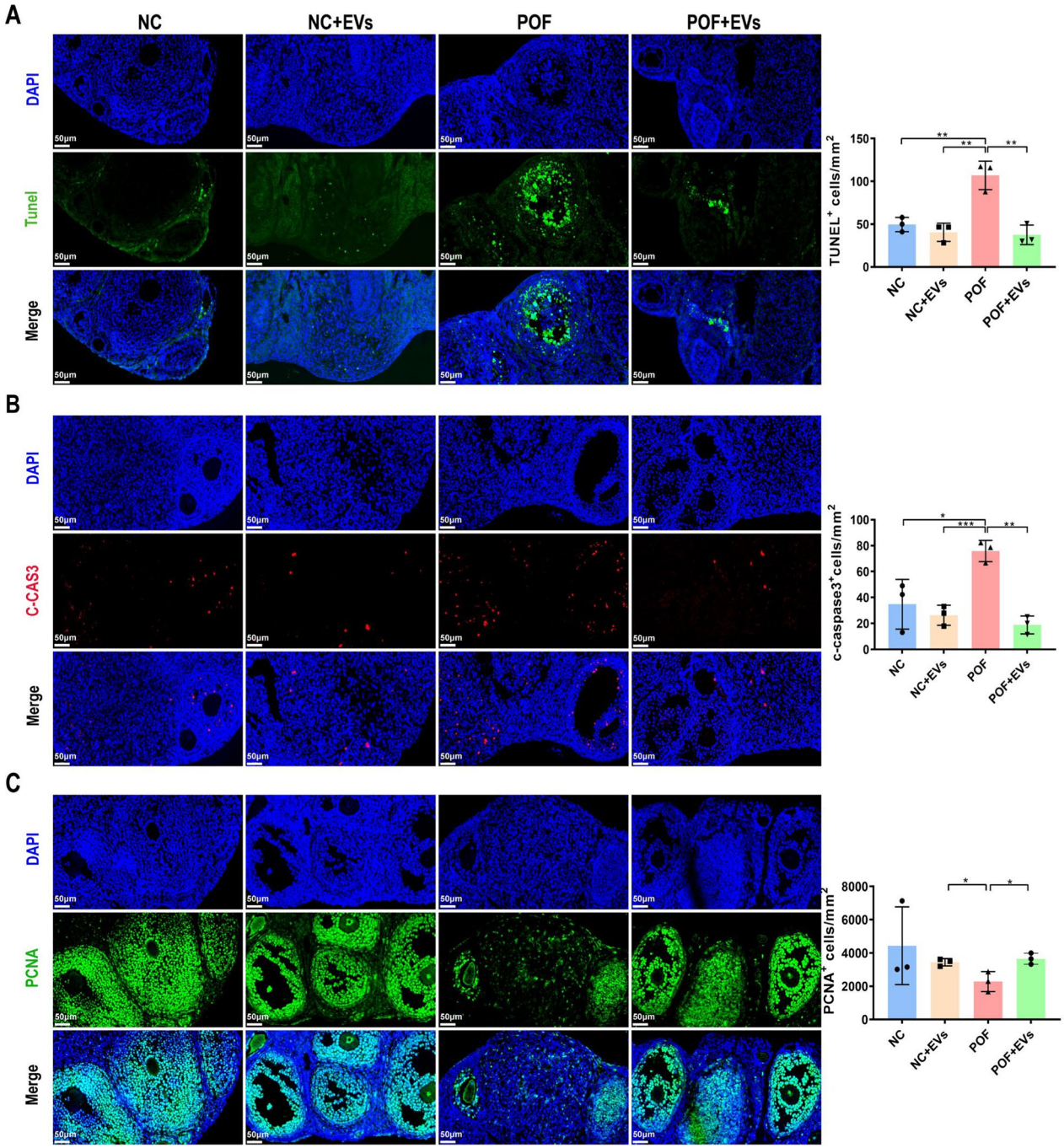

Fig. 7 The anti-apoptotic and pro-proliferative effects of EVs derived from UC-MSCs in POF. **A** Representative images and quantification of TUNEL staining. Scale bar: 50 μm. **B** Representative images and quantification of cleaved-caspase3 immunofluorescence staining. Scale bar: 50 μm. **C** Representative images and quantification of PCNA immunofluorescence staining. Scale bar: 50 μm. $^{*}p < 0.05$, $^{**}p < 0.01$, $^{***}p < 0.001$. $n = 3$ per group for all experiments

NM + GW4869-CM, 47.1 ± 3.5% vs. 31.6 ± 5.1%) (Fig. 8F). Our findings suggested that UC-MSC-derived EVs not only inhibit NM-induced apoptosis but also promote the proliferation of KGN cells, and that the PI3K/AKT signaling pathway might be involved in these processes.

Proteomic analysis of UC-MSC-derived EVs

The quantitative proteomics analysis showed that 728 proteins were identified in the proteomes of control medium samples and EVs from human UC-MSCs, among which 522 proteins were significantly upregulated

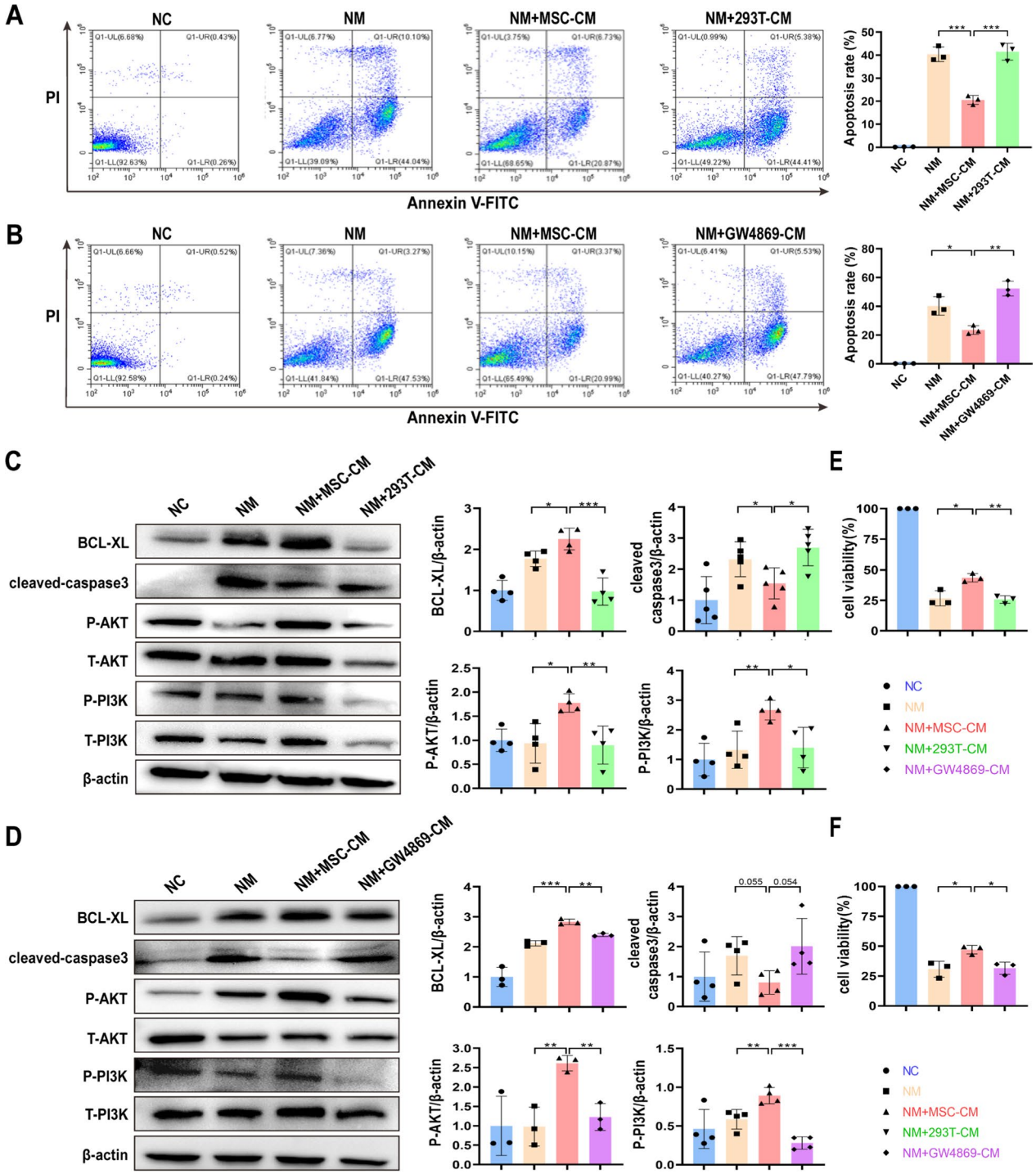

Fig. 8 EVs from UC-MSCs inhibited apoptosis and promoted proliferation of KGN cells. **A**, **B** The KGN cells apoptosis detected by flow cytometry. **C**, **D** The expression of apoptosis-related proteins and proteins related to the PI3K/AKT signaling pathway in KGN cells detected by Western blot analysis. All full-length blots are presented in Additional file 2: Figure 8C and D. **E**, **F** CCK8 assay for proliferation of KGN cells. *$p < 0.05$, **$p < 0.01$, ***$p < 0.001$

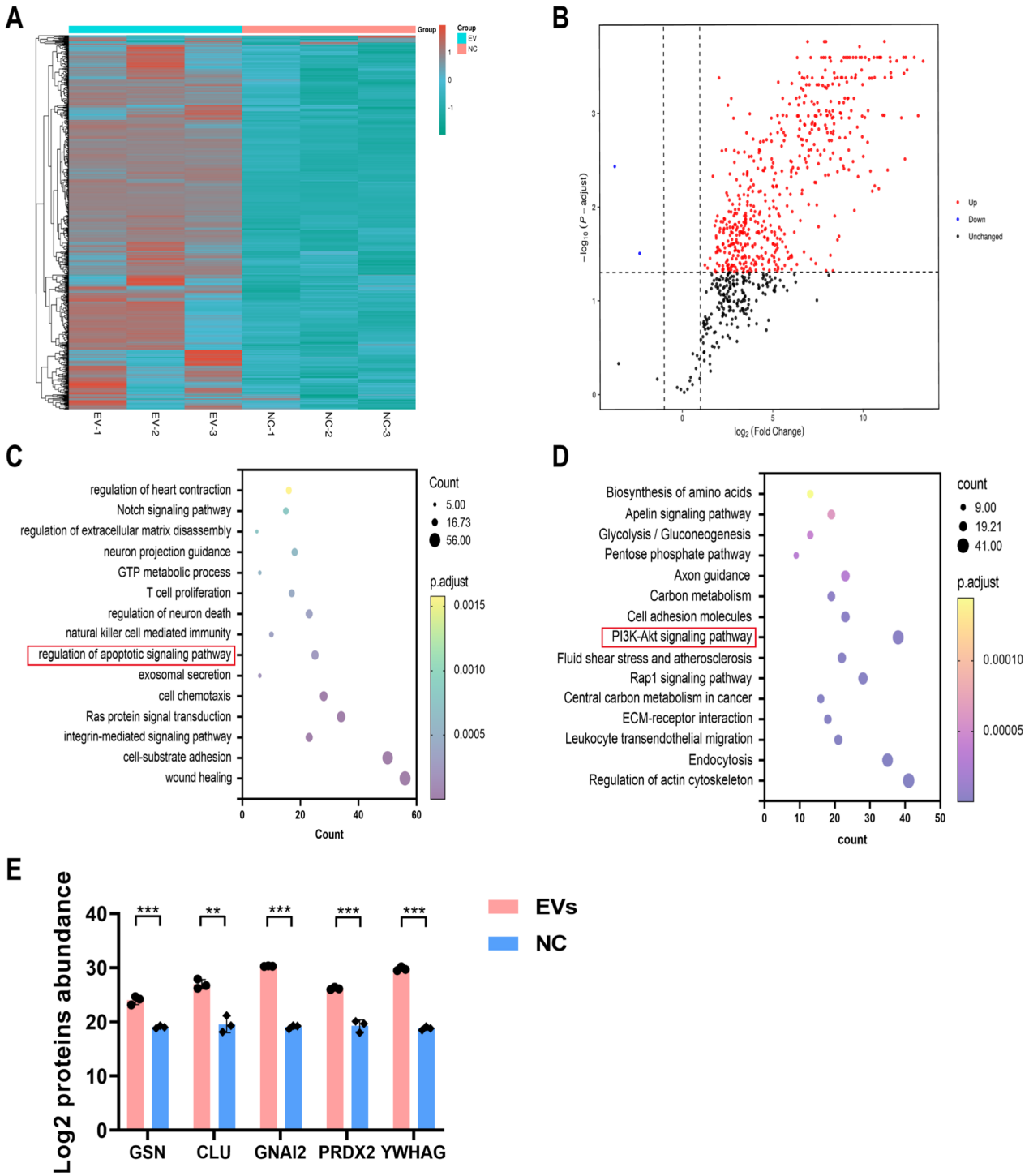

Fig. 9 Label-free quantitative proteomics comparison of UC-MSCs-derived EVs and NC medium samples. **A** Heat map of differential expression proteins in EVs and control medium. **B** Volcano plot of differential expression proteins in EVs and control medium. The red points indicated higher protein expression in the EVs and blue points indicated lower protein expression in the EVs compared to the control medium. **C** GO enrichment analysis of biological process. **D** KEGG pathway enrichment analysis. **E** Log2 proteins abundance of GSN, CLU, GNAI2, PRDX2 and YWHAG. $^{**}p < 0.01$, $^{***}p < 0.001$

and 2 proteins were significantly downregulated in EVs (Fig. 9A and B). GO enrichment analysis annotated biological process in which the identified proteins were involved. Notably, the regulation of apoptotic signaling pathway was closely related to the efficacy of EVs on POF (Fig. 9C). Moreover, the KEGG analysis indicated significant enrichment of the PI3K/AKT signaling pathway, which was associated with 38 proteins (Fig. 9D). The five anti-apoptotic proteins that differed significantly from the control medium, including CLU, Gelsolin (GSN), Guanine nucleotide-binding protein G(i) subunit alpha-2 (GNAI2), Peroxiredoxin-2 (PRDX2) and 14-3-3 protein gamma (YWHAG), may play key regulatory roles in the inhibition of apoptosis by EVs (Fig. 9E).

CLU of UC-MSCs-derived EVs inhibited apoptosis and promoted proliferation in KGN cells by activating the PI3K/AKT pathway

The protein expression of CLU, GSN, GNAI2, PRDX2 and YWHAG in UC-MSCs was inhibited significantly by siRNA transfection (Fig. S1A). Flow analysis results indicated that the downregulation of CLU expression by siRNA significantly impaired the anti-apoptotic effect of MSC-CM (NM + siNC-CM vs. NM + siCLU-CM, 19.4 ± 0.33% vs. 27.0 ± 1.6%) (Fig. 10A). Consistently, treatment with exogenous CLU proteins also significantly inhibited NM-induced apoptosis in KGN cells (NM vs. NM + CLU-100 ng/mL, 30.1 ± 2.9% vs. 19.7 ± 1.2%) (Fig. 10B). By contrast, the downregulation of GSN, GNAI2, PRDX2 and YWHAG expression in UC-MSCs did not affect NM-induced apoptosis of KGN cells (Fig. S1B). When CLU was down-regulated in UC-MSCs, the ability of MSC-CM to regulate BCL-XL and cleaved-caspase3 in KGN cells was suppressed (Fig. 10C). We next investigated whether CLU of UC-MSCs-EVs had anti-apoptotic effect on KGN cells through the PI3K/AKT pathway. The relative protein expression levels of p-PI3K and p-AKT were decreased with CLU knockdown (Fig. 10C). CCK8 results showed that knockdown of CLU downregulated the proliferative effect of MSC-CM on KGN cells (NM + siNC-CM vs. NM + siCLU-CM, 70.6 ± 7.0% vs. 56.5 ± 7.5%) (Fig. 10D). Likewise, exogenous CLU proteins had a pro-proliferative effect over KGN cells (NM vs. NM + CLU-100 ng/mL, 35.4 ± 13.0% vs. 61.3 ± 9.2%) (Fig. 10E). Taken together, our findings demonstrated that CLU from UC-MSCs-derived EVs inhibited apoptosis and promoted proliferation of ovarian granulosa cells by activating the PI3K/AKT pathway.

Discussion

In this study, we found that mice exhibit ovarian failure after 9 days of intraperitoneal injections with CTX/BUS. Treatment of POF mice with human UC-MSCs and EVs derived from UC-MSCs on day 6 was able to significantly improve ovarian function in chemotherapy-induced ovarian damage. Meanwhile, human UC-MSCs and EVs had anti-apoptotic and pro-proliferative effects on ovarian granulosa cells in vivo and in vitro. Further mechanistic studies showed that CLU of EVs derived from human UC-MSCs inhibited apoptosis and promoted proliferation of ovarian granulosa cell through activating the PI3K/AKT pathway.

POF is a disorder with multiple causative factors, including genetic factors, autoimmune disorders, chemotherapy and/or radiotherapy, as well as environmental pollutants [16, 21, 22]. POF is one of the sequelae of cytotoxic chemotherapy among young female with cancer. CTX and BUS are the most commonly used alkylating agent antitumor drugs. Apoptosis of ovarian cells, ovarian cortex fibrosis and depletion of ovarian reserve have been reported to be involved in chemotherapy induced POF [18, 23, 24]. To investigate the pathological changes of POF induced by chemotherapeutic agents, we examined the number of follicles, hormone levels, cell apoptosis and fibrosis in POF and NC mice every three days after injection of CTX with BUS until day 21. Our results revealed that the mice treated with CTX/BUS exhibited a significant loss of primordial follicles on day 6, and a significant reduction in the number of follicles at all stages on day 9, compared with the control group. On the other hand, the number of atretic follicles in POF mice was significantly increased on day 3. The previous studies reported that the mechanism of follicle depletion involves increased recruitment of primordial follicles into the growing pool and induction of apoptotic death in growing follicles [25]. Here, we observed that the primordial follicle depletion was earlier than primary and secondary follicles. Our data further support that reduction of the primordial pool can arise indirectly via the loss of activated and/or growing follicles. In addition, the apoptosis of ovarian granulosa cells in POF mice was significantly increased and maintained high levels 3 days after CTX/BUS injection, but no signs of fibrosis were observed within 21 days. We demonstrate here that on day 9 after CTX/BUS injection, mice developed significant ovarian failure, which was closely associated with the apoptosis of ovarian granulosa cells.

Ovarian tissue cryopreservation with subsequent transplantation is one of the means for female fertility preservation [26]. However, this treatment carries the risk of carrying malignant cells [23]. HRT could suppress menopausal symptoms but barely improve reproductive functions of the ovaries [27, 28]. In recent years, MSCs-based therapies have been reported to be effective in treating POF [13, 28, 29]. UC-MSCs have no ethical difficulties and can be easily obtained in comparison to

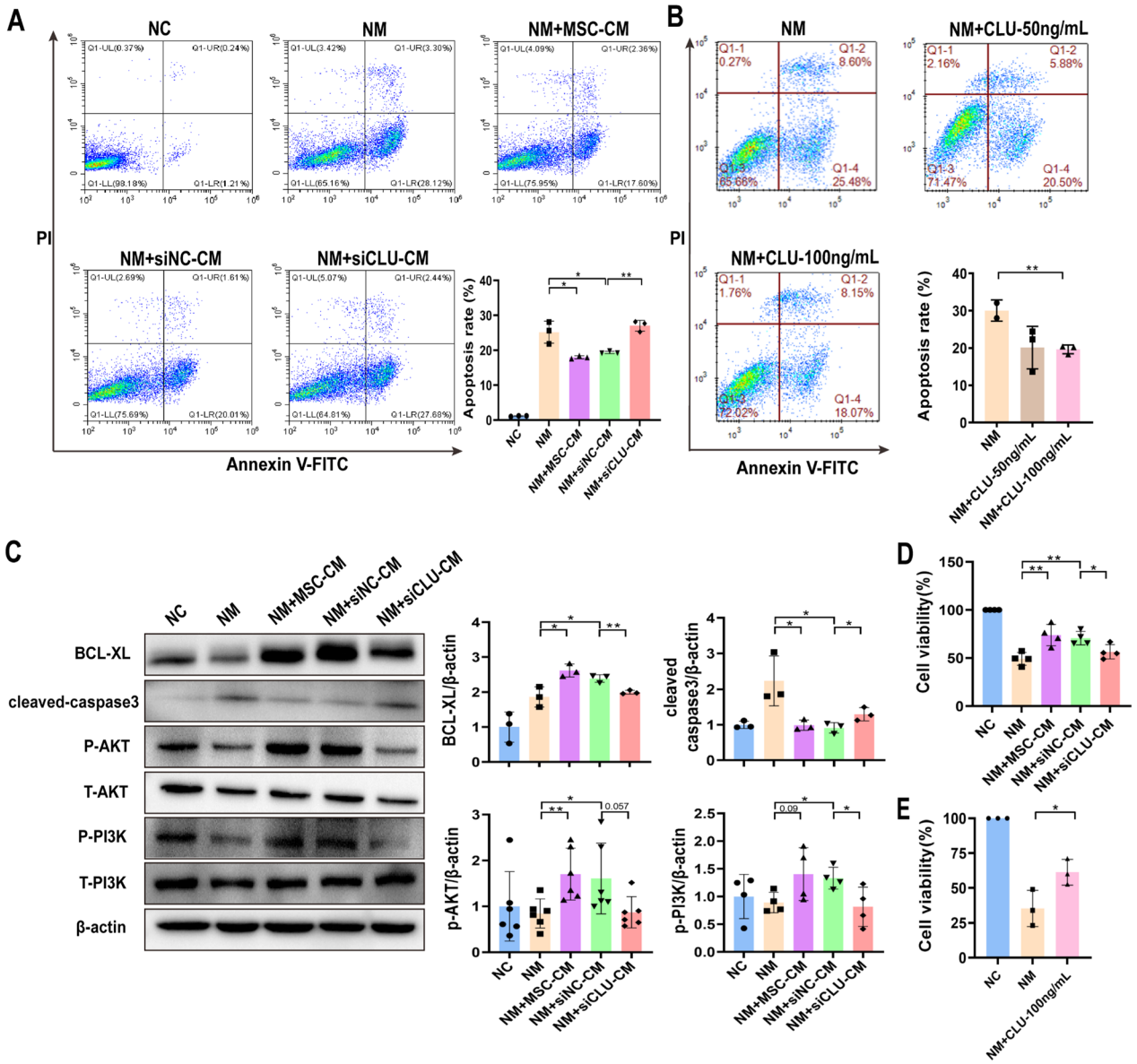

Fig. 10 CLU of UC-MSCs-derived EVs inhibited apoptosis and promoted proliferation of KGN cells. **A**, **B** The effect of siCLU-CM and exogenous CLU proteins on KGN cell apoptosis were detected by flow cytometry. **C** Western blot analysis was performed to detect the effects of MSC-CM after knockdown of CLU on the expression of apoptosis-related proteins and proteins related to the PI3K/AKT signaling pathway in KGN cells. All full-length blots are presented in Additional file 2: Figure 10C. **D**, **E** CCK8 assay to detect the effect of MSC-CM after knockdown of CLU and exogenous CLU proteins on KGN cell proliferation. *$p < 0.05$, **$p < 0.01$

other sources of stem cells. Several studies showed that human UC-MSCs transplantation restores ovarian function by inhibiting apoptosis, improving lipid metabolism and alleviating excessive autophagy [13, 18, 30]. However, the timing of human UC-MSCs treatment is a critical factor determining the recovery of ovarian function, further studies are required to explore the appropriate timing. Based on the pathological changes observed in POF, the current study administered human UC-MSCs to mice via tail vein injection on crucial time points of days 6, 9, and 12 to investigate their potential therapeutic effects. POF mice that were injected with UC-MSCs on day 6 significantly increased the number of primordial, primary and secondary follicles, and inhibited follicle atresia. We observed increased numbers of primordial and secondary follicles, but the number of primary and atretic follicles did not significantly change in POF mice treated with UC-MSCs on day 9. Notably, no significant differences in

follicle numbers were observed in POF mice treated with UC-MSCs on day 12. Correspond with previous studies [12], human UC-MSCs inhibited ovarian cell apoptosis and promoted proliferation. However, we further found that there was no anti-apoptosis and pro-proliferative effect when UC-MSCs were administered on days 9 and 12. These results suggest that the timing of UC-MSCs injections is critical for therapeutic intervention.

Numerous studies have demonstrated that paracrine mechanisms are critical in human UC-MSCs-mediated improvement of ovarian function [17, 31]. Here, we isolated EVs to investigate the role of EVs derived from human UC-MSCs in POF. The results showed that EVs derived from human UC-MSCs inhibited apoptosis and restored the ovarian structures and function in chemotherapy-induced POF mice. Meanwhile, we observed that EVs promoted cell proliferation in ovaries. Previously, Eslami et al. have shown that injecting POF mice with 400 μg of EVs derived from bone marrow MSCs improved ovarian function and restored fertility [32]. Another study by Xiao et al. indicated that intra-ovarian injection of amniotic fluid stem cell-derived exosomes (125 μg) was adequate to alleviate ovarian injury in chemotherapy-induced POF mice [33]. In our study and previous studies, the timing, doses, and treatment approaches of EVs differed significantly among protocols. The doses of EVs were lower and the treatment approach was simpler in our study compared to those used in previous studies. Meanwhile, our results regarding the optimal timing of human UC-MSCs treatment in POF help to ascertain the timing for EVs treatment as well. In vitro, our data suggested that the apoptosis of NM-damaged KGN cells was significantly inhibited after treatment with UC-MSCs supernatant. Meanwhile, the proliferation of KGN was significantly enhanced after coculture with human UC-MSCs supernatant. However, there was no similar effect when KGNs were cocultured with 293T-CM. In addition, when exosome secretion of human UC-MSCs was suppressed by GW4869, the anti-apoptosis and pro-proliferative effects of UC-MSC supernatant was weakened. These results demonstrate that UC-MSC-derived EVs have the anti-apoptosis and pro-proliferative effects, like UC-MSCs. However, there are still numerous issues that need to be resolved for their successful clinical application. There is no internationally accepted standardized method for the high-throughput, high-purity, and minimal damage separation of EVs from cell culture medium [34]. Furthermore, the heterogeneity of EVs poses one of the main challenges in current clinical EVs studies.

EVs can regulate the function of target cells by transferring reparative proteins, mRNAs, lncRNAs and miRNAs. Hu et al. proposed that human UC-MSCs derived EVs can regulate bone metabolism by transferring CLEC11A [35]. Previous studies have shown that exosomal miRNA (eg, miR-22-3p and miR126-3p) from human UC-MSCs repair ovarian injury and improve ovarian function [17, 18]. However, there are few studies on bioactive proteins of EVs for the treatment of POF induced by chemotherapeutic agents. To test the critical functional molecules, label-free quantitative proteomics was performed to detect proteins in EVs derived from human UC-MSCs. With the label-free quantitative proteomics, 522 cellular proteins levels were significantly upregulated in EVs. GO enrichment analysis showed that biological processes of these proteins were involved in apoptotic signaling pathways. The CLU is a glycosylated protein that involved in a variety of physiological processes, including apoptotic cell death, lipid transport and DNA repair [36]. Some studies have suggested that CLU can protect against cardiomyocytes and podocytes from oxidative stress-induced apoptosis [37, 38]. You et al. found that CLU expression could promote ovarian cancer cell proliferation and resistance to cisplatin [39]. To our knowledge, the effect of CLU in POF has not been reported so far. In this study, our data indicated that CLU was highly enriched in EVs of human UC-MSCs. CLU knockdown was found to attenuate the protective effect of UC-MSC-derived EVs on KGN cells apoptosis. Meanwhile, the pro-proliferative effect of EVs was arrested when CLU was inhibited. We could not determine whether knockdown of CLU with siRNA in human UC-MSCs might affect the expression of other genes to affect the regulatory effects of EVs. Therefore, the anti-apoptosis and pro-proliferative effect of CLU was validated by the use of recombinant CLU proteins. Additionally, Hou et al. proposed that CLU replenishment may alleviate cell death, which supports our findings in the study [40]. Indeed, engineered EVs loaded with additional amounts of CLU will further prove our conclusion. This will be corroborated in our follow-up studies.

It is well known that the PI3K/AKT pathway plays an important role in regulating autophagy, apoptosis, proliferation and follicular growth [30, 41]. It has been reported that exosomes derived from human UC-MSCs could restore damaged ovarian function through the PI3K/AKT pathway [18]. As expected, our findings provided evidence that the supernatants of UC-MSCs enriched with EVs modulated the PI3K/AKT pathway in ovarian granulosa cells. Evidence suggested CLU could inhibit senescence and inflammation through activation of PI3K/AKT pathway [42, 43]. Therefore, we hypothesized that CLU could play a role in POF by activating the PI3K/AKT signaling pathway. In the present study, we revealed that phosphorylation of PI3K and AKT was significantly inhibited in KGN cells after

knockdown of CLU. These results indicated that EVs derived from UC-MSCs could alleviate apoptosis and promote proliferation via CLU-mediated PI3K/AKT activation. In addition, an in-depth study of the mechanisms of CLU-mediated activation of multiple signaling pathways is important for enhancing the therapeutic potential of UC-MSCs-derived EVs and the translation capacity into clinic. These questions will be given priority in our future studies.

Conclusion

In this study, we explored the appropriate timing of UC-MSCs treatment for POF. Our findings suggested that UC-MSCs treatment on day 6 effectively ameliorated ovarian structure and function in POF mice. The EVs derived from UC-MSCs have similar effects as UC-MSCs in improving ovarian function in POF mice. Importantly, our preliminary study demonstrated for the first time that CLU from UC-MSCs-derived EVs can inhibit apoptosis and promote proliferation of ovarian granulosa cells through activating the PI3K/AKT pathway. Further studies are required to clarify whether CLU-overexpressed UC-MSCs can enhance the efficacy of ovarian function improvement in POF, which may pave the way for the use of gene-modified cell therapy for POF.

Abbreviations

POF	Premature ovarian failure
FSH	Follicle-stimulating hormone
E2	Estradiol
HRT	Hormone replacement therapy
UC-MSCs	Human umbilical cord-derived mesenchymal stem cells
EVs	Extracellular vesicles
MSC-CM	UC-MSCs conditioned medium
NTA	Nanoparticle tracking analysis
HE	Hematoxylin and eosin
BSA	Bovine serum albumin
PCNA	Proliferating cell nuclear antigen
TUNEL	TdT mediated dUTP nick end labeling
DMEM	Dulbecco's modified Eagle's medium
FBS	Fetal bovine serum
siRNA	Small interfering RNA
SDS-PAGE	Sodium dodecyl sulfate–polyacrylamide gel electrophoresis
PVDF	Polyvinylidene difluoride
GO	Gene Ontology
KEGG	Kyoto encyclopedia of genes and genomes

Supplementary Information

The online version contains supplementary material available at https://doi.org/10.1186/s13287-024-03926-7.

Additional file 1: **Fig. S1 The knockdown efficiency by qPCR assay and the effect of these supernatant on KGN apoptosis.** (A) The mRNA levels of CLU, GSN, GNAI2, PRDX2 and YWHAG after transfection with siRNA in UC-MSCs. (B) The effect of supernatant after siRNA transfection of UC-MSCs on apoptosis of KGN cells detected by flow cytometry. **p < 0.01, ***p < 0.001.

Additional file 2

Acknowledgements

This work was supported by grants from the Wuhan Municipal Science and Technology Bureau (Grant No. 2023020402010771); the Innovation and Entrepreneurship Leading Team Project in Zengcheng District, Guangzhou (Grant No. 202001002); Key Research and Development Plan of Hubei Province (Grant No. 2021BCA134); and Key Research Project of Wuhan Donghu New Technology Development Zone (Grant No. 2022KJB118).

Author contributions

JH performed in vivo and in vitro experiments, and data analysis; CA, ML, TD, SZ and KZ performed in vivo experiments; CT, YO, RL, YJ and YY performed in vitro experiments; CL and DW conceived and supervised the study, and critically revised the manuscript. All authors read and approved the final manuscript.

Availability of data and materials

All data generated and/or analyzed during this study are included in this published article. The mass spectrometry proteomics data have been deposited to the ProteomeXchange Consortium (https://proteomecentral.proteomexchange.org) via the iProX partner repository [44, 45] with the dataset identifier PXD052006 (URL: https://www.iprox.cn/page/PSV023.html;?url=1715563210770kX9Q. Password: nC7z).

Declarations

Ethics approval and consent to participate

The research project was conducted according to the ARRIVE guidelines (Animal Research: Reporting of In Vivo Experiments). The animal studies were approved by the Committee of Animal Care and Use at Hubei Provincial Center for Food and Drug Safety Evaluation and Animal Experiment (Project title: The mechanism research of human umbilical cord mesenchymal stem cells and extracellular vesicles against chemotherapeutic drug-induced premature ovarian failure. The Permit Number: 202210022. Feb 23, 2022) and approved by the Bestcell Model Biological Center Notification of the Result for Ethical Approval for Research Involving Animals (Project title: Reach of pathological process of premature ovarian failure model induced by chemotherapy. The permit Number: BSMS 2022-06-27A. JUN 27, 2022). UC-MSCs were obtained following informed, written patient consent, and the approval was obtained by the Institutional Ethics Review Board of Renmin Hospital of Wuhan University (Project title: Clinical study of human umbilical cord mesenchymal stem cells for the treatment of diabetic nephropathy. The permit Number: WDRY2019-G001. Nov 22, 2019).

Consent for publication

Not applicable.

Competing interests

The authors declare that there is no conflict of interest regarding the publication of this paper.

Author details

[1]Department of Biochemistry and Molecular Biology, Wuhan University School of Basic Medical Sciences, Wuhan, China. [2]College of Life Sciences, Hubei University, Wuhan, China. [3]Reproductive Medicine Center, Tongji Hospital, Tongji Medical College, Huazhong University of Science and Technology, Wuhan, China. [4]R&D Center, Wuhan Hamilton Biotechnology Co., Ltd, Wuhan, China. [5]Department of Oncology, Nanfang Hospital, Southern Medical University, Guangzhou, China. [6]Department of Physiology, Wuhan University School of Basic Medical Sciences, Wuhan, China. [7]Xianning Medical College, Hubei University of Science and Technology, Xianning, China. [8]R&D Center, Guangzhou Hamilton Biotechnology Co., Ltd, Guangzhou, China.

Received: 30 April 2024 Accepted: 5 September 2024
Published online: 13 September 2024

References

1. Christianson MS, Wodi P, Talaat K, et al. Primary ovarian insufficiency and human papilloma virus vaccines: a review of the current evidence. Am J Obstet Gynecol. 2020;222(3):239–44.
2. De Vos M, Devroey P, Fauser BC. Primary ovarian insufficiency. Lancet. 2010;376(9744):911–21.
3. Sheikhansari G, Aghebati-Maleki L, Nouri M, et al. Current approaches for the treatment of premature ovarian failure with stem cell therapy. Biomed Pharmacother. 2018;102:254–62.
4. Yang M, Lin L, Sha C, et al. Bone marrow mesenchymal stem cell-derived exosomal miR-144-5p improves rat ovarian function after chemotherapy-induced ovarian failure by targeting PTEN. Lab Invest. 2020;100(3):342–52.
5. Lin RJ, Wang T. Comparison of fundamental frequency in postmenopausal women who are treated with hormone replacement therapy vs those who are not: a systematic review and meta-analysis. JAMA Otolaryngol Head Neck Surg. 2020;146(11):1045–53.
6. Beral V, Banks E, Reeves G. Evidence from randomised trials on the long-term effects of hormone replacement therapy. Lancet. 2002;360(9337):942–4.
7. Huang B, Qian C, Ding C, et al. Fetal liver mesenchymal stem cells restore ovarian function in premature ovarian insufficiency by targeting MT1. Stem Cell Res Ther. 2019;10(1):362.
8. Zhang S, Zhu D, Mei X, et al. Advances in biomaterials and regenerative medicine for primary ovarian insufficiency therapy. Bioact Mater. 2021;6(7):1957–72.
9. Huang Y, Ma Z, Kuang X, et al. Sodium alginate-bioglass-encapsulated hAECs restore ovarian function in premature ovarian failure by stimulating angiogenic factor secretion. Stem Cell Res Ther. 2021;12(1):223.
10. Yin N, Wu C, Qiu J, et al. Protective properties of heme oxygenase-1 expressed in umbilical cord mesenchymal stem cells help restore the ovarian function of premature ovarian failure mice through activating the JNK/Bcl-2 signal pathway-regulated autophagy and upregulating the circulating of CD8(+)CD28(-) T cells. Stem Cell Res Ther. 2020;11(1):49.
11. Zafardoust S, Kazemnejad S, Darzi M, et al. Intraovarian administration of autologous menstrual blood derived-mesenchymal stromal cells in women with premature ovarian failure. Arch Med Res. 2023;54(2):135–44.
12. Deng T, He J, Yao Q, et al. Human umbilical cord mesenchymal stem cells improve ovarian function in chemotherapy-induced premature ovarian failure mice through inhibiting apoptosis and inflammation via a paracrine mechanism. Reprod Sci. 2021;28(6):1718–32.
13. Zhao Y, Ma J, Yi P, et al. Human umbilical cord mesenchymal stem cells restore the ovarian metabolome and rescue premature ovarian insufficiency in mice. Stem Cell Res Ther. 2020;11(1):466.
14. Chen B, Li Q, Zhao B, et al. Stem cell-derived extracellular vesicles as a novel potential therapeutic tool for tissue repair. Stem Cells Transl Med. 2017;6(9):1753–8.
15. Yang W, Zhang J, Xu B, et al. HucMSC-derived exosomes mitigate the age-related retardation of fertility in female mice. Mol Ther. 2020;28(4):1200–13.
16. Zhang Q, Sun J, Huang Y, et al. Human amniotic epithelial cell-derived exosomes restore ovarian function by transferring microRNAs against apoptosis. Mol Ther Nucleic Acids. 2019;16:407–18.
17. Gao T, Chen Y, Hu M, et al. MicroRNA-22-3p in human umbilical cord mesenchymal stem cell-secreted exosomes inhibits granulosa cell apoptosis by targeting KLF6 and ATF4-ATF3-CHOP pathway in POF mice. Apoptosis. 2023;28(7–8):997–1011.
18. Qu Q, Liu L, Cui Y, et al. miR-126-3p containing exosomes derived from human umbilical cord mesenchymal stem cells promote angiogenesis and attenuate ovarian granulosa cell apoptosis in a preclinical rat model of premature ovarian failure. Stem Cell Res Ther. 2022;13(1):352.
19. Bahrehbar K, Rezazadeh Valojerdi M, Esfandiari F, et al. Human embryonic stem cell-derived mesenchymal stem cells improved premature ovarian failure. World J Stem Cells. 2020;12(8):857–78.
20. Lv X, Guan C, Li Y, et al. Effects of single and multiple transplantations of human umbilical cord mesenchymal stem cells on the recovery of ovarian function in the treatment of premature ovarian failure in mice. J Ovarian Res. 2021;14(1):119.
21. Domniz N, Meirow D. Premature ovarian insufficiency and autoimmune diseases. Best Pract Res Clin Obstet Gynaecol. 2019;60:42–55.
22. Vabre P, Gatimel N, Moreau J, et al. Environmental pollutants, a possible etiology for premature ovarian insufficiency: a narrative review of animal and human data. Environ Health. 2017;16(1):37.
23. Khaleghi S, Eivazkhani F, Tavana S, et al. Follicular reconstruction and neo-oogenesis in xenotransplantation of human ovarian isolated cells derived from chemotherapy-induced POF patients. J Biol Eng. 2023;17(1):70.
24. Sun L, Li D, Song K, et al. Exosomes derived from human umbilical cord mesenchymal stem cells protect against cisplatin-induced ovarian granulosa cell stress and apoptosis in vitro. Sci Rep. 2017;7(1):2552.
25. Luderer U, Lim J, Ortiz L, et al. Exposure to environmentally relevant concentrations of ambient fine particulate matter (PM(2.5)) depletes the ovarian follicle reserve and causes sex-dependent cardiovascular changes in apolipoprotein E null mice. Part Fibre Toxicol. 2022;19(1):5.
26. Azevedo AR, Pais AS, Almeida-Santos T, et al. Medical grade honey as a promising treatment to improve ovarian tissue transplantation. Bioengineering. 2022;9(8):357.
27. Sassarini J, Lumsden MA, Critchley HO. Sex hormone replacement in ovarian failure—new treatment concepts. Best Pract Res Clin Endocrinol Metab. 2015;29(1):105–14.
28. Ai G, Meng M, Guo J, et al. Adipose-derived stem cells promote the repair of chemotherapy-induced premature ovarian failure by inhibiting granulosa cells apoptosis and senescence. Stem Cell Res Ther. 2023;14(1):75.
29. Li X, Li C, Tang Y, et al. NMDA receptor activation inhibits the antifibrotic effect of BM-MSCs on bleomycin-induced pulmonary fibrosis. Am J Physiol Lung Cell Mol Physiol. 2018;315(3):L404–21.
30. Dai W, Yang H, Xu B, et al. Human umbilical cord-derived mesenchymal stem cells (hUC-MSCs) alleviate excessive autophagy of ovarian granular cells through VEGFA/PI3K/AKT/mTOR pathway in premature ovarian failure rat model. J Ovarian Res. 2023;16(1):198.
31. Li Z, Zhang M, Tian Y, et al. Mesenchymal stem cells in premature ovarian insufficiency: mechanisms and prospects. Front Cell Dev Biol. 2021;9:718192.
32. Eslami N, Bahrehbar K, Esfandiari F, et al. Regenerative potential of different extracellular vesicle subpopulations derived from clonal mesenchymal stem cells in a mouse model of chemotherapy-induced premature ovarian failure. Life Sci. 2023;321:121536.
33. Xiao GY, Cheng CC, Chiang YS, et al. Exosomal miR-10a derived from amniotic fluid stem cells preserves ovarian follicles after chemotherapy. Sci Rep. 2016;6:23120.
34. Yu D, Li Y, Wang M, et al. Exosomes as a new frontier of cancer liquid biopsy. Mol Cancer. 2022;21(1):56.
35. Hu Y, Zhang Y, Ni CY, et al. Human umbilical cord mesenchymal stromal cells-derived extracellular vesicles exert potent bone protective effects by CLEC11A-mediated regulation of bone metabolism. Theranostics. 2020;10(5):2293–308.
36. Shannan B, Seifert M, Leskov K, et al. Challenge and promise: roles for clusterin in pathogenesis, progression and therapy of cancer. Cell Death Differ. 2006;13(1):12–9.
37. He J, Dijkstra KL, Bakker K, et al. Glomerular clusterin expression is increased in diabetic nephropathy and protects against oxidative stress-induced apoptosis in podocytes. Sci Rep. 2020;10(1):14888.
38. Jun HO, Kim DH, Lee SW, et al. Clusterin protects H9c2 cardiomyocytes from oxidative stress-induced apoptosis via Akt/GSK-3beta signaling pathway. Exp Mol Med. 2011;43(1):53–61.
39. You J, Han Y, Qiao H, et al. Hsa_circ_0063804 enhances ovarian cancer cells proliferation and resistance to cisplatin by targeting miR-1276/CLU axis. Aging. 2022;14(11):4699–713.
40. Hong JY, Kim MN, Kim EG, et al. Clusterin deficiency exacerbates hyperoxia-induced acute lung injury. Cells. 2021;10(4):944.
41. Ming-Yan Y, Jing Z, Shu-Qin G, et al. Liraglutide inhibits the apoptosis of human nucleus pulposus cells induced by high glucose through PI3K/Akt/caspase-3 signaling pathway. Biosci Rep. 2019;39(8):BSR20190109.
42. Ungsudechachai T, Honsawek S, Jittikoon J, et al. Clusterin exacerbates interleukin-1beta-induced inflammation via suppressing PI3K/Akt pathway in human fibroblast-like synoviocytes of knee osteoarthritis. Sci Rep. 2022;12(1):9963.
43. Zhang Y, Zhang Y, Xiao Y, et al. Expression of Clusterin suppresses Cr(VI)-induced premature senescence through activation of PI3K/AKT pathway. Ecotoxicol Environ Saf. 2019;183:109465.
44. Chen T, Ma J, Liu Y, et al. iProX in 2021: connecting proteomics data sharing with big data. Nucleic Acids Res. 2022;50(D1):D1522–7.

45. Ma J, Chen T, Wu S, et al. iProX: an integrated proteome resource. Nucleic Acids Res. 2019;47(D1):D1211–7.

Publisher's Note